IEEE Access
Multidisciplinary ⋮ Rapid Review ⋮ Open Access Journal

Received 2 February 2024, accepted 7 April 2024, date of publication 16 April 2024, date of current version 23 April 2024.

Digital Object Identifier 10.1109/ACCESS.2024.3389962

RESEARCH ARTICLE

Path Generation Based on Electrostatic Equipotential Curves

CHUNGWEI LIN[1], YEBIN WANG[1], (Senior Member, IEEE), WILLIAM T. VETTERLING[1], (Life Member, IEEE), DEVESH K. JHA[1], (Senior Member, IEEE), AND RIEN QUIRYNEN[1,2]

[1]Mitsubishi Electric Research Laboratories (MERL), Cambridge, MA 02139, USA
[2]Stack AV, Pittsburgh, PA 15106, USA

Corresponding author: Chungwei Lin (clin@merl.com)

ABSTRACT Path planning for a point-mass robot moving in a cluttered two-dimensional environment is a well studied but non-trivial problem. In this paper we propose a novel computationally efficient and resolution-complete path generation method based on electrostatics. The proposed scheme comprises two stages. First, an auxiliary electrostatic problem is formulated where the boundary conditions of the Laplace equation are specified based on the map of the original path planning problem and is solved to obtain a map-specific electrostatic potential. Second, feasible paths are constructed by following any equipotential curve whose potential value is different from those of obstacles and boundaries. The electrostatic potential in the proposed method differs from the celebrated repulsive/attractive force-based potential field by its non-vanishing gradient, based on which the resolution-completeness is established. The computational efficiency of the proposed method arises from a novel electrostatic solver based on complex analysis, and on an original collision-checking algorithm inspired by the Residue theorem. Extensive numerical examples are provided to demonstrate the effectiveness and limitations of the proposed method. We believe this work provides an unconventional strategy for quantitatively encoding global map information and can play a role complementary to prevailing path planning methods.

INDEX TERMS Complex analysis, electric potential solver, path planning.

I. INTRODUCTION

Path planning, meaning the generation of a feasible path to a target position while avoiding all obstacles in the environment, is a classic and fundamental problem in robotics. It is typically the first requirement for applications such as autonomous driving, robotic motion planning, etc. [1], [2], [3]. This problem has been extensively studied in the past several decades and numerous results have been presented. Established methods include Rapidly-exploring Random Tree (RRT) [4], [5], [6], [7], [8], [9], [10], [11], Probabilistic RoadMap (PRM) [12], [13], [14], [15], [16], Potential Field based methods [17], [18], [19], [20], [21], [22], Bug algorithms [23], [24], [25], A* [26] and its variants [27], [28], [29], [30], and visibility or tangent graph [31], [32], to name a few. Despite being an area of active research for decades, this problem remains open in several ways.

Completeness guarantee and computational efficiency are two main objectives of any path planning scheme, but it is generally difficult to design algorithms having both features simultaneously. For example, sampling-based methods are complete and can even provide some asymptotic optimality guarantees, but they become inefficient for pathological cases such as for maps with narrow passages. Graph-based methods, such as A*, rely on estimated ''cost-to-go'' to guide the search. As encoding the map information into cost-to-go is very challenging, A* could be misguided and thus suffers from low computation efficiency. Potential Field methods are computationally efficient, but the searching process can be trapped in local minima and therefore cannot be complete. Due to non-convexity of collision-free configuration space, most of the optimization-based path planning methods struggle to find feasible solutions in cluttered environments [33], [34].

The associate editor coordinating the review of this manuscript and approving it for publication was Su Yan.

Most of prior path generation methods make use of only local map information, even if all obstacles are given. For example, both sampling-based and visibility-based methods use global information to generate collision-free samples, while planning is done by searching over neighboring points. The Potential Field approach regards each obstacle as a short-ranged repulsive potential whose strength decays exponentially away from the obstacles. Indeed it is not obvious whether the obstacles and boundaries far away could affect the local path planning, and if one developed a procedure to include these effects, what the benefits could be. This is the very aspect that this work attempts to explore.

This paper presents a computationally efficient and resolution-complete path planning method in a two-dimensional (2D) space by means of an innovative use of the global map information. The proposed method breaks the path planning into two sub-problems. In the first sub-problem, an auxiliary electrostatic problem is setup based on the map, and solved for the electrostatic potential. Specifically, boundaries and obstacles are represented by perfect metals, with boundaries carrying different amounts of charge whereas obstacles are charge neutral. A highly efficient electrostatic potential solver is developed via the use of complex analytical functions [35], [36], [37]. In the second sub-problem, feasible (collision-free) paths are constructed by exploiting the electrostatic potential as a roadmap or graph. In particular using the property that each metallic surface has a constant potential, feasible paths can be generated by following any equipotential curve whose potential value is different from those of all obstacles and boundaries. Each feasible path is labeled by a potential within the known upper and lower bounds; multiple topologically non-equivalent paths can be generated by scanning the potential values. Associating each path with a finite scalar value is a manifestation of quantitative utilization of global information. We regard this as the most distinctive feature compared to other existing methods. Major advantages of the proposed method are three-fold: 1) resolution-completeness; 2) flexibility to construct a family of collision-free paths parameterized by the potential value; and 3) computation and memory efficiency. The practical limitations of our method can be traced to the numerical resolution, and can be circumvented by performing a few additional calculations. This paper considers only a point-mass robot for clarity of presentation. The geometric size of the robot can be treated by inflating/shrinking the obstacles/boundaries.

The rest of this paper is organized as follows. Section II is devoted to a brief literature review. Section III defines the problem and outlines the proposed approach. Section IV is dedicated to formulating and solving the auxiliary electrostatic problem for an electrostatic potential field. Section V details how path construction is done by using the electrostatic potential field. Section VI establishes the resolution-completeness of the proposed method, addresses the limitations and corresponding remedies, and discusses the differences to the Potential Field approach. In Section VII two examples are presented. In Section VIII we consider two alternative boundary conditions that could be useful for specific tasks. Brief conclusions are given in Section IX. In the Appendix we provide details for the developed 2D electrostatic potential solver. As a general comment on notation, in this paper we use complex numbers to represent 2D points and vectors: $Z = X + iY$ or $z = x + iy$ denotes a point. A vector $\mathbf{E} = [E_x, E_y]^\top \in \mathbb{R}^2$ is represented by $E = E_x + iE_y$ and can be normalized as $\hat{E} = E/|E|$.

II. RELATED WORK

There have been several different approaches presented for the path planning and motion planning problems. We briefly review a few known path generation schemes that are relevant to the proposed method.

The Potential Field approach [17], [18], [19], [20], [21], [22] constructs a potential field that has a higher value at the initial point and a lower value at the target point. A feasible path is generated by following the gradient of the potential field. The potential in our scheme is different from the potential in Potential Field approach, and we shall make a detailed comparison in Section VI-C.

Graph-based path generation schemes contain two main steps: (i) constructing a graph (i.e., points and connections) that covers at least one feasible path; (ii) connecting neighboring points to create a feasible path. Sample-based methods generate a graph/tree by randomly sampling the collision-free points. Well-established sampling-based algorithms for graph construction include PRM [12], RRT [6], etc. Interested readers are referred to [38] for more information. The Visibility-based method [31], [32] deterministically uses the vertices of polygonal obstacles to construct a graph. Once a graph is given, feasible paths subject to some optimization criterion such as shortest distance or energy minimum [4], [13], [28] are generated. The potential in our scheme plays a role very similar to the graph.

The Bug algorithm [23], [24], [25], which is shown to be complete, implements the following rule: when encountering an obstacle, circle around the obstacle and leave it at the point closest to the target point. The Bug algorithm is fast as it does not require graph construction, but it cannot easily generate multiple paths. A part of our proposed path generation is similar to the Bug algorithm, but with the criterion to leave an obstacle depending on the obtained potential field.

The problem becomes much more complicated when taking the robot dynamics into account. Generally the energy-optimal/time-optimal collision-free motion planning can be categorized into decomposition-based [39] and kinodynamic approaches [40]. The former divides the problem into a purely geometric path generation part and a dynamics-related motion planning part, whereas the latter deals with both simultaneously and is usually more computationally demanding. More involved techniques such as the minimum principle [41], [42], dynamic programming [43], numerical optimization [44], [45], [46], and Mixed-Integer Linear

Programming [47] have been used to find the feasible/optimal solution. This aspect is not considered in this work.

III. PROBLEM STATEMENT AND ALGORITHM OUTLINE

This section defines the path planning problem and outlines the proposed algorithm.

A. PROBLEM STATEMENT

A configuration $\mathbf{q}$ of a robot is a minimum-dimension parameterization which uniquely defines the positions of all points on the robot. The configuration space, including all possible configurations, is denoted as $\mathcal{C}$. A configuration $\mathbf{q}$ is collision-free if the robot at $\mathbf{q}$ does not overlap with obstacles in the environment. The set of all collision-free configurations is denoted $\mathcal{C}_{\text{free}} \subset \mathcal{C}$.

This work considers a point-mass robot which moves in a compact set $\mathcal{D}$ of the global 2D plane where

$$\mathcal{D} \triangleq [x_{\min}, x_{\max}] \times [y_{\min}, y_{\max}] \subset \mathbb{R}^2. \tag{1}$$

Here $x_{\min}, x_{\max}, y_{\min}, y_{\max}$ are constants. The robot configuration $\mathbf{q}$ has a parameterization: (x, y). The robot is confined in the region of interest specified by

$$\mathcal{D}_{\text{ROI}} \triangleq \{\mathbf{q} \mid \mathbf{q} \in \mathcal{D}, f_1(\mathbf{q}) > 0, f_2(\mathbf{q}) > 0\}, \tag{2}$$

where $f_1(x, y) > 0$ and $f_2(x, y) > 0$ further restrict the workspace of the robot. For example $f_1(x, y) = 0$ and $f_2(x, y) = 0$ can be used to represent two boundaries of a non-straight passage. Note that $f_1(x, y) = 0$ and $f_2(x, y) = 0$ do not necessarily lie within $\mathcal{D}$, in which case, $\mathcal{D}$ and $\mathcal{D}_{\text{ROI}}$ are the same. If $\mathcal{D}_{\text{ROI}}$ is the rectangular area as specified in (1), we can take either $f_1(x, y) = x - x_{\min}$ and $f_2(x, y) = x_{\max} - x$ or $f_1(x, y) = y - y_{\min}$ and $f_2(x, y) = y_{\max} - y$.

Remark 1: Constraints $f_1 = 0$ and $f_2 = 0$ represent *two* boundaries that are needed to define the boundary conditions of the electrostatic problem in Section IV-A. In the case that there is no physical restriction on the workspace other than $\mathcal{D}$, one can introduce $f_1(x, y), f_2(x, y)$ as virtual boundaries. □

Denote the region occupied by the ith obstacle $\mathcal{D}_{\text{obs},i}$. The collision-free configuration is given by

$$\mathcal{C}_{\text{free}} = \mathcal{D}_{\text{ROI}} \setminus \cup_{i=1}^{n_{\text{obs}}} \mathcal{D}_{\text{obs},i} \tag{3}$$

where n_{obs} is the number of obstacles. For simplicity, the information $\{\mathcal{D}, f_1, f_2, \mathcal{D}_{\text{obs},i} \text{ for } 1 \le i \le n\}$ is named after the *map*. Given the definitions of map and configuration, we are ready to state the path planning problem as follows.

Problem 2: Given the initial configuration $\mathbf{q}_{\text{init}} \in \mathcal{C}_{\text{free}}$ and the target configuration $\mathbf{q}_{\text{target}} \in \mathcal{C}_{\text{free}}$; find a path $\mathcal{P} : [0, 1] \to \mathcal{C}_{\text{free}}$ which starts at $\mathbf{q}_{\text{init}}$ and ends at $\mathbf{q}_{\text{target}}$.

As the analytical properties of complex functions will be used to solve for the electrostatic potential field, it is convenient to use complex numbers to represent the robot configurations. A complex number Z equivalently represents the robot configuration $\mathbf{q} \in \mathbb{R}^2$ and forms a space $\mathbb{C}$ where $\mathbb{C} = \{x + iy | x, y \in \mathbb{R}\}$. Using complex numbers,

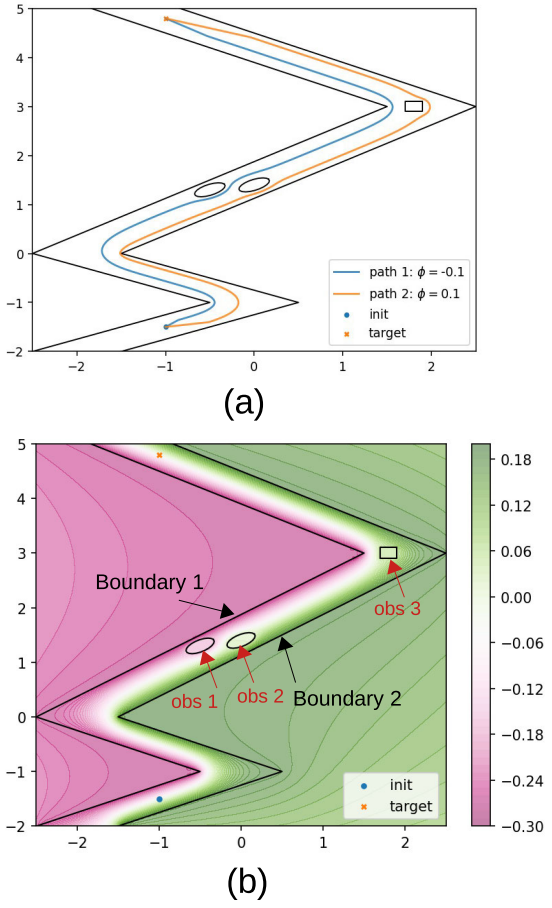

FIGURE 1. (a) Problem illustration. Two elliptical and one rectangular obstacles are between two zig-zag boundaries. The initial and target points are respectively represented by the dot and cross. The goal is to find a path that connects the initial and target points, stays between two boundaries, and avoids all obstacles. Two feasible paths, obtained by the proposed scheme, are given. (b) For the auxiliary electrostatic problem, +1/-1 charge are placed on the right/left zig-zag boundaries respectively whereas three obstacles are charge neutral. The resulting potential (color scale) and equipotential curves are used for generating feasible paths. Path 1 and Path 2 shown in (a) correspond to $\Phi = -0.1$ and $\Phi = 0.1$ respectively.

Problem 2 is solved over complex space: the initial and target points are respectively represented by $Z_{\text{init}} = X_{\text{init}} + iY_{\text{init}}$, $Z_{\text{target}} = X_{\text{target}} + iY_{\text{target}}$; a feasible path $\mathcal{P}$ is represented by a collection of complex numbers $\mathcal{P} = (Z_{\text{init}}, z_1, z_2, \cdots, Z_{\text{target}})$.

B. OUTLINE OF PATH GENERATION SCHEME

Problem 2 is divided into two sub-problems. First, we relate a given map to an auxiliary electrostatic problem and solve for a potential field. Second, the resulting potential field is used as a graph (roadmap) to construct feasible paths. The proposed path planning method is outlined in Algorithm 1: steps 1-2 correspond to the first sub-problem and is discussed in Section IV; steps 3-5 correspond to the second sub-problem and is elaborated in Section V.

Equipotential curve in Alg. 1 has the following definition.

Algorithm 1: Equipotential-Based Path Generation

1. Given a map, setup an auxiliary electrostatic problem by regarding obstacles and boundaries as conductors, and assigning opposite charges to two boundaries.
2. Solve the auxiliary electrostatic problem for the 2D electrostatic potential.
3. Pick a potential Φ_{ref} which is different from the potentials of any obstacles, and computes its equipotential curve, denoted as $C(\Phi_{\text{ref}})$.
4. Construct a path $\mathcal{P}_1$ connecting Z_{init} to a point $Z_{\text{ref},1} \in C(\Phi_{\text{ref}})$; construct a path $\mathcal{P}_2$ connecting a point $Z_{\text{ref},2} \in C(\Phi_{\text{ref}})$ to Z_{target}.
5. Concatenate $\mathcal{P}_1$, $C(\Phi)$, $\mathcal{P}_2$ to obtain one feasible path $\mathcal{P}(\Phi_{\text{ref}})$.

Definition 3: Let $\Phi(X, Y)$ be the potential of an electric vector field $\mathbf{E}(X, Y) = -\nabla\Phi(X, Y)$, the level curve $\Phi(X, Y) = C$, denoted by $C(\Phi)$, is called the Equipotential Curve or the Contour.

C. ILLUSTRATIVE EXAMPLE

Fig.1(a) illustrates how Alg. 1 is applied to construct a path from initial point $Z_{\text{init}} = -1 - 1.5\,i$ to target point $Z_{\text{target}} = -1 + 4.8\,i$. The map is characterized by $\mathcal{D} \triangleq [-2.5, 2.5] \times [-2, 5]$; f_1 and f_2 for the two zig-zag boundaries #1 and #2, respectively; and three obstacles.

First, the auxiliary electrostatic problem is setup and solved for the electrostatic potential which is shown as a color map in Fig.1(b). Then, the potential is used as a roadmap or a graph to construct feasible paths. Each feasible path contains an equipotential curve and can be labeled by its potential value. In this example, path 1 and path 2 shown in Fig. 1(a) correspond to $\Phi_{\text{ref}} = -0.1$ and $\Phi_{\text{ref}} = 0.1$, respectively.

IV. ELECTROSTATIC POTENTIAL FIELD

In this section we elaborate how to setup the auxiliary electrostatic problem and highlight relevant features that will be used in path generation.

A. AUXILIARY ELECTROSTATIC PROBLEM

Given a map for Problem 2, i.e., $\mathcal{D}_{\text{ROI}}$ and all obstacles $\cup_{i=1}^{n_{\text{obs}}} \mathcal{D}_{\text{obs},i}$, the auxiliary electrostatic problem is setup as follows: boundaries and obstacles are regarded as perfect conductors; charges of +1/-1 are placed on the two boundaries, respectively, whereas the obstacles are charge neutral. The electrostatic potential $\Phi(X, Y)$ in $\mathcal{D}_{\text{ROI}}$ satisfies the Laplace equation

$$\left[\frac{\partial^2}{\partial X^2} + \frac{\partial^2}{\partial Y^2}\right]\Phi(X, Y) = 0. \tag{4}$$

Remark 4: Assigning the total charge on each conductor determines the 2D electrostatic potential up to a position-independent constant and uniquely determines the electric field [48]. Charge assignment is equivalent to specifying the boundary conditions for the Laplace equation. Positions of initial and target points are not part of the boundary conditions and thus do not affect the resulting potential field. That is: the potential field is fully determined by the map, and can be treated as a roadmap for both single- and multi-query uses. □

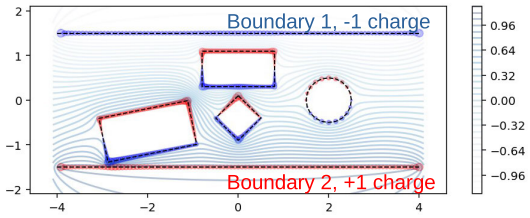

FIGURE 2. Potential contours, obtained by a 2D potential solver, are needed for the path generation scheme. In this example, charges of -1 and +1 are placed on the top and bottom line boundaries, respectively. A few charge neutral conductors, which will represent obstacles in the proposed path generation method, are placed between these two boundaries. Notice that the potential is a constant over the area occupied by a conductor. The dots indicate the surface charge distributions (with size representing amplitude, and the colors red/blue representing sign.) Each boundary has a constant potential.

B. THE 2D POTENTIAL SOLVER

We develop an efficient 2D potential solver for the auxiliary electrostatic problem. Detailed procedures, benchmarks, and distinct advantages are detailed in the Appendix. A representative result is shown in Fig. 2, where charges of -1 and $+1$ are respectively placed on the top and bottom line boundaries, and all obstacle-related conductors are charge neutral. Because charges are free to move inside the conductor, a static solution is only possible when the charges of each conductor adjust themselves such that each conductor has a constant potential and thus zero electric field. This is seen in Fig. 2 where equipotential curves do not enter any of the conductors (up to numerical errors).

C. IMPORTANT FEATURES

We list four general features of the electrostatic potential that are crucial to path construction.

- (F1): all points within a metallic object have the same potential. This implies that boundaries and obstacles, albeit spatially extended, can be described by their corresponding potential values.
- (F2): the potential is defined over the entire Z-plane. If only two of objects carry opposite charges, the potential over the entire plane is bounded by the potentials of these two objects. Denote the potentials at upper and lower boundaries as $\Phi_{\text{b},1}$, $\Phi_{\text{b},2}$, and that at ith obstacle as $\Phi_{\text{obs},i}$ which satisfies

$$\Phi_{\text{b},1} < \Phi_{\text{obs},i} < \Phi_{\text{b},2}. \tag{5}$$

As described in the Appendix, the solver provides the potential Φ and its gradient $\mathbf{E} = -\nabla\Phi$ efficiently. Both quantities are important in our path generation scheme.

- (F3): any equipotential curve $C(\Phi)$ is collision-free as long as Φ is different from $\Phi_{\text{b},1}$, $\Phi_{\text{b},2}$ and $\Phi_{\text{obs. }i}$.
- (F4): within the region between the two boundaries, i.e. $\mathcal{D}_{\text{ROI}}$, the potential has no local extrema or saddle points. In other words, the gradient $\mathbf{E} = -\nabla\Phi$ is non-zero everywhere in the collision-free region.

Remark 5: Generally, points of the same potential can belong to two disconnected contours. The auxiliary electrostatic potential problem setup prevents this from happening by imposing charge-neutrality on obstacles, ruling out local extrema or saddle points from the potential Φ in the region of interest $\mathcal{D}_{\text{ROI}}$. □

Remark 6: A complex function $F(Z) = F_R(X, Y) + iF_I(X, Y)$ has real and imaginary parts. In the proposed solver we solve for a complex $\Phi(Z)$ whose real part represents the electrostatic potential, i.e., $\text{Re}[\Phi(Z)] = \Phi(X, Y)$. To simplify the notation, $\Phi(Z)$ should be understood to refer to the potential $\Phi(X, Y)$ for the remainder of this paper. □

V. PATH GENERATION BASED ON EQUIPOTENTIAL CURVES

In this section, we complete our path generation method by elaborating steps that solve the second sub-problem: how to generate feasible paths given the potential $\Phi(Z)$. We also provide an efficient and robust 2D collision checking method based on complex analysis.

A. EQUIPOTENTIAL-BASED PATH CONSTRUCTION

Steps 1-2 in Alg. 1 result in an electrostatic potential field $\Phi(Z)$ and have been discussed in Section IV-B. Given the electrostatic potential field $\Phi(Z)$ for $Z \in \mathcal{D}_{\text{ROI}}$, we follow Steps 3-5 in Alg. 1 to construct a path from Z_{init} to Z_{target}.

In Step 3: one picks any potential $\Phi_{\text{ref}} \in (\Phi_{\text{b},1}, \Phi_{\text{b},2}) \backslash \Phi_{\text{obs}}$ where $\Phi_{\text{obs}} \triangleq \{\Phi_{\text{obs},1}, \cdots, \Phi_{\text{obs},n_{\text{obs}}}\}$ and determines the equipotential curve $C(\Phi_{\text{ref}})$. An equipotential curve is generated by following the direction (denoted as $\hat{T} \equiv (E_y - iE_x)/|\mathbf{E}|$) that is perpendicular to the potential gradient (which is $\hat{E} \equiv (E_x + iE_y)/|\mathbf{E}|$). As shown in Fig. 3, to find the next equipotential point of Z_i, we first propose $Z'_{i+1} = Z_i \pm \hat{T}(Z_i)|\text{d}Z|$ with $|\text{d}Z|$ a chosen stepsize. To eliminate the discretization error caused by $|\text{d}Z|$, we perform a one-dimensional search on the line segment between $Z'_{i+1} \pm \hat{E}(Z_i)|\text{d}Z|$ to find the next equipotential point

$$Z_{i+1} = \text{argmin}_Z \big[\Phi(Z_i) - \Phi(Z)\big]^2, \quad \text{with } Z \in Z'_{i+1} + \alpha\hat{E}(Z_i)|\text{d}Z|,\ |\alpha| < 1. \tag{6}$$

Note that $\pm\hat{T}$ are both allowed.

In Step 4: we connect the initial point and the target point to $C(\Phi_{\text{ref}})$ without crossing any obstacles or boundaries, i.e., constructing paths $\mathcal{P}_1$ and $\mathcal{P}_2$ in Alg. 1. Paths $\mathcal{P}_1$ and $\mathcal{P}_2$ usually cross equipotential curves. To construct them, we recognize the fact that the potential has no local extrema and propose to follow the gradient direction to move downstream (if $\Phi(Z_{\text{init}}) > \Phi_{\text{ref}}$) or upstream ($\Phi(Z_{\text{init}}) < \Phi_{\text{ref}}$). Once hitting an obstacle, the equipotential curve is followed until reaching a point at which following the gradient direction once again avoids obstacles. As shown in Fig. 4, the procedure involves three scenarios: (i) following the gradient consistent with the potential difference; (ii-a) when the proposed point using (i) hits an obstacle, then following the transverse direction; (ii-b) if the point proposed by (ii-a) hits an obstacle, then adding a gradient component to bring the path back to $\mathcal{C}_{\text{free}}$. Again there are two directions in which to follow the equipotential curve; we keep both as long as they each stay within the region of interest. For numerical stability, we avoid saddle points resulting from discretization error by choosing a minimum field strength $E_{\min}$ below which one follows the equipotential curve. $E_{\min}$ is chosen to be much smaller than the electric field defined by $\frac{|\Phi_{\text{b},1} - \Phi_{\text{b},2}|}{L}$ where L is the distance between two boundaries.

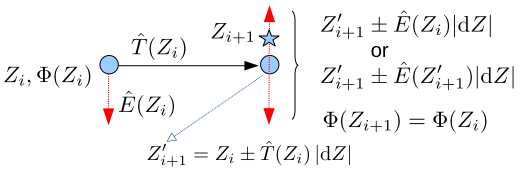

FIGURE 3. Procedure to generate a contour from Z_i (left circle) to Z_{i+1} (star). The contour is generated by two steps: first following the transverse direction (denoted as $\hat{T}$), the direction perpendicular to the potential gradient (along the electric field, denoted as $\hat{E}$), to Z_{i+1} (right circle); second to perform a line search along $\hat{E}$ to find the equilpotential point. Note that the transverse directions has two options and we keep both paths as long as they stay within the region of interest.

The final feasible path is a concatenation of (i) a curve connecting Z_{init} and $Z_{\text{ref},1}$, (ii) the contour $C(\Phi_{\text{ref}})$ between $Z_{\text{ref},1}$ and $Z_{\text{ref},2}$, and (iii) a curve connecting $Z_{\text{ref},2}$ and Z_{target}. (i) and (iii) will be referred to as the "downstream" or "upstream" parts of the path whereas (ii) is the equipotential part of the path. $Z_{\text{ref},1}$ and $Z_{\text{ref},2}$ are not unique, and one can post-process a feasible path to make it smoother and shorter.

Remark 7: Due to the concatenation, a generated path $\mathcal{P}$ is usually piece-wise smooth. Using $\mathcal{P}$ as the starting point, the trajectory can be smoothed with well-established interpolation methods using, for example, Bézier Curves [49] or B-splines [50]. □

Each feasible path $P_{\text{f}}(\Phi_{\text{ref}})$ is parameterized by a potential value Φ_{ref}. It is collision-free because $\Phi_{\text{ref}} \notin \Phi_{\text{obs}}$ and the ith obstacle has a constant potential $\Phi_{\text{obs},i}$; it is confined between two boundaries because $\Phi_{\text{b},1} < \Phi_{\text{ref}} < \Phi_{\text{b},2}$. The stepsize $|\text{d}Z|$, which nearly appears in all path generation schemes, is a tuning parameter: $|\text{d}Z|$ has to be sufficiently small for the scheme to work, but using a larger $|\text{d}Z|$ reduces the computation time. In practice we start with a $|\text{d}Z|$ that is much shorter than the characteristic scale of any obstacles, and may gradually increase its value after trials.

B. RESIDUE THEOREM-BASED COLLISION CHECK

Many path planning schemes, including the proposed one, require a robust and efficient procedure to check whether a point Z lies inside or outside a polygon, the boundary of which is represented by a sequence of ordered points

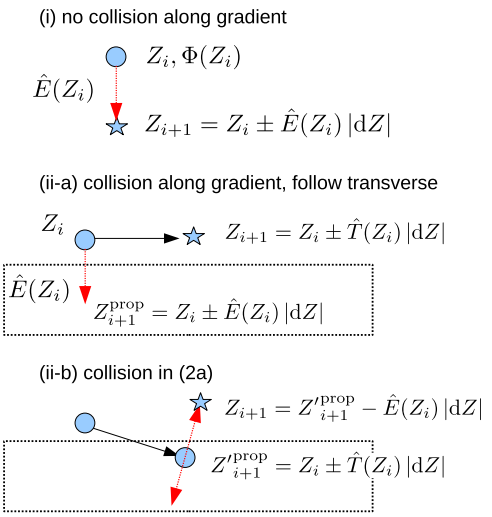

FIGURE 4. Procedure to connect two points of different potentials. To connect two points of different potentials, first follow the steepest direction (i), i.e., either the steepest ascent or descent. If following this gradient hits a obstacle, then one follows the transverse direction (ii-a). If (ii-a) hits a obstacle, then we add a small gradient component to bring it back into the allowed region. Note that the transverse directions has two options and we keep both paths as long as they stay within the region of interest.

$(z_0, z_1, \cdots, z_{n-1}, z_n = z_0)$. This can be done by utilizing the residue theorem, i.e., the point Z satisfies

$$\frac{1}{2\pi i}\oint \frac{\mathrm{d}z}{z-Z} = \frac{1}{2\pi i}\sum_{i=0}^{n-1}\log\left[\frac{z_{i+1}-Z}{z_i-Z}\right] = \begin{cases} 1 & Z \text{ inside the polygon} \\ 0 & Z \text{ outside the polygon.} \end{cases} \tag{7}$$

Eq. (7) assumes a counter-clockwise ordering of $\{z_i\}$. We can remove this consideration by using the absolute value of the integral. Eq. (7) can deal with any polygon, convex or not, and is particularly efficient when specifying a large obstacle using only a few vertices. The computation efficiency of (7) stems from the analytical expression whereas the robustness comes from the binary output; it is used in all path finding schemes in this paper.

Eq. (7) can also be used to examine the topological equivalence of two feasible paths. Consider two feasible paths:

$$\begin{aligned} \mathcal{P}_1 &= (z_0^{(1)} = Z_{\mathrm{init}}, z_1^{(1)}, \cdots, z_{n-1}^{(1)}, z_n^{(1)} = Z_{\mathrm{target}}) \\ \mathcal{P}_2 &= (z_0^{(2)} = Z_{\mathrm{init}}, z_1^{(2)}, \cdots, z_{m-1}^{(2)}, z_m^{(2)} = Z_{\mathrm{target}}), \end{aligned} \tag{8}$$

where their concatenation results in a closed loop, denoted as $\mathcal{L}_{1-2}$. To check if two paths are topologically equivalent or not, we compute

$$T_{1-2}^{(j)} = \frac{1}{2\pi i}\oint_{\mathcal{L}_{1-2}} \frac{\mathrm{d}z}{z-Z_j} = \frac{1}{2\pi i}\left[\sum_{i=0}^{n-1}\log\frac{z_{i+1}^{(1)}-Z_j}{z_i^{(1)}-Z_j} - \sum_{i=0}^{m-1}\log\frac{z_{i+1}^{(2)}-Z_j}{z_i^{(2)}-Z_j}\right] \tag{9}$$

where Z_j is any point inside the jth obstacle. $|T_{1-2}^{(j)}|$ is either zero or one. The former implies that the two paths are topologically equivalent with respect to the jth obstacle, i.e., the two paths can continuously deform to each other without crossing the jth obstacle. The latter implies topological non-equivalence, i.e., continuously deforming one path to the other forces it to cross the jth obstacle.

VI. ANALYSIS

This section provides analysis of the proposed method. We first show that under some assumptions our method is complete. We then examine the scenarios in which the proposed scheme can run into numerical difficulty and discuss how to get around them. Finally a detailed comparison with the Potential Field approach is presented to highlight the distinct features of our method.

A. COMPLETENESS

In this subsection the Cartesian coordinate (X, Y) (instead of the complex number $Z = X + iY$) is used to represent the location.

Proposition 8: Alg.1 is resolution-complete.

As long as there exists a feasible path, Alg. 1 can find one if the auxiliary electrostatic potential problem is solved exactly. However, in order to balance computation and memory efficiency, the potential field solution to the auxiliary electrostatic potential problem has a limited resolution. Thus Alg. 1 is resolution-complete.

Lemma 9: Given any $\Phi_0 \in (\Phi_{\mathrm{b},1}, \Phi_{\mathrm{b},2})$ and $\Phi_0 \notin \Phi_{\mathrm{obs}}$, the contour $\Phi(X, Y) = \Phi_0$ is not a closed curve in $\mathcal{D}_{\mathrm{ROI}}$.

Proof: Assume $\Phi(X, Y) = \Phi_0$ is a closed curve, and intersects with a straight line at (X_1, Y_1) and (X_2, Y_2). Along the straight line $(X(t), Y(t)) = (X_1, Y_1) + t(X_2 - X_1, Y_2 - Y_1)$ with $t \in [0, 1]$, there has to be a local minimum or maximum because $\Phi(X, Y)$ is continuous. This leads to a contradiction with the feature (F4), and thus the assumption is invalid. ■

Lemma 10: Contour $\Phi(X, Y) = \Phi_0$ in $\mathcal{D}_{\mathrm{ROI}}$ with $\Phi_0 \notin \Phi_{\mathrm{obs}}$ and $\Phi_0 \in (\Phi_{\mathrm{b},1}, \Phi_{\mathrm{b},2})$ is unique.

Proof: From Lemma 9, all contours $\Phi(X, Y) = \Phi_0$ with $\Phi_0 \notin \Phi_{\mathrm{obs}}$ are not closed curves and thus intersect with the boundaries of $\mathcal{D}_{\mathrm{ROI}}$. Assume $\Phi(X, Y) = \Phi_0$ has two different contours, denoted as $C_1(\Phi_0)$ and $C_2(\Phi_0)$, and $(X_1, Y_1) \in C_1(\Phi_0)$ and $(X_2, Y_2) \in C_2(\Phi_0)$. Along the straight line $(X(t), Y(t)) = (X_1, Y_1) + t(X_2 - X_1, Y_2 - Y_1)$ with $t \in [0, 1]$, there has to be a local minimum or maximum because $\Phi(X, Y)$ is continuous. Because $\Phi(X, Y)$ has no local extrema in $\mathcal{D}_{\mathrm{ROI}}$, the assumption cannot be true. ■

Given Lemmas 9 -10 and the feature (F4), Proposition 8 is shown below.

Proof: As stated in Step 5, our generated path contains three parts: one upstream, one equipotential, and one downstream. The equipotential connects two points of the same potential by following the contour, i.e., by the direction perpendicular to the gradient. From Lemma 10, the contour of a given potential is *unique*. The upstream/downstream segments are constructed by following the gradient (when away from obstacles) and following the equipotential (when colliding with an obstacle). Because there are no local

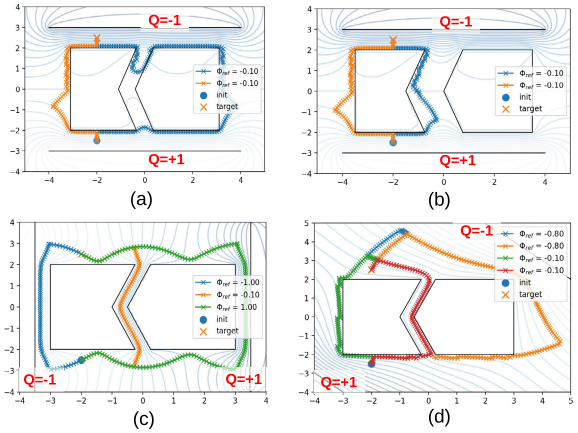

FIGURE 5. Limitations due to small gradients and heuristics from electrostatics:. (a) When the middle gap is narrow and two boundaries are horizontal, the potential around the gap is almost constant (vanishing gradient) and our scheme cannot identify it. (b) when the gap becomes wider, the potential has some distribution and our scheme identifies the gap as a feasible path. (c) and (d): the same gap as (a) but placing two boundaries along the vertical directions and with a 45° rotation. In these setups the gradient around the gap is strong enough that the scheme can identify the gap as one of feasible paths. Boundary charges of each case are indicated in red.

extremal, this procedure is guaranteed to work in principle. ■

B. LIMITATIONS AND REMEDY STRATEGIES

Alg. 1 suffers from two types of numerical issues, both of which can be traced back to the resolution of the potential field. First, due to the discretization error the potentials inside each conductor are not strictly constant but have a very weak spatial dependence. This is explicitly seen in Fig. 5(a) and (b) where some equipotential curves penetrate into obstacles. This issue becomes more pronounced if the obstacle boundary has large or even diverging curvature. A straightforward remedy to this issue is to increase the number of points around the high-curvature part of the obstacle boundary. Alternatively one can choose a feasible path $\mathcal{P}(\Phi)$ whose potential value excludes the small potential range of the obstacle.

The other numerical issue arises from the small gradient. This issue also originates from resolution, as ideally the zero gradient only occurs inside the conductors. If a feasible path passes through a region of very small gradient, our path search algorithm may not be able to follow it, as the vanishing gradient does not provide sufficient guidance. This usually happens for a long narrow gap, where the feasible path is sandwiched by two large obstacles. Fig. 5 provides a series of examples. As seen in Fig. 5(a), when the gap is narrow and the two boundaries are horizontal, the potential over the gap is almost constant and the corresponding gradient is close to zero. In this case our scheme does not find the path going through the gap. When the gap becomes wider, as shown in Fig. 5(b), the potential inside the gap has a more significant spatial distribution, and thus larger variations, and our scheme then identifies the gap as a feasible path. We stress that it is the vanishing gradient, not necessarily the narrowness of allowed space, that prevents our solver from identifying the feasible path. As shown in Fig. 5(c) where the gap width is identical to that of Fig. 5(a), by placing the two boundaries vertically one gets a larger gradient along the gap. In this case, all three topologically non-equivalent feasible paths are found.

In the proposed method, an equipotential curve is always collision-free. The numerically challenging part is to connect two points of different potential [Step 4 in Section V-A]. When there are no obstacles between two points of different potentials, Step 4 can easily be achieved by following the gradient. Otherwise the path must include both an equipotential part to avoid obstacles, and upstream/downstream parts to match the beginning and ending potentials. Vanishing gradients may cause numerical problems in this process. Given a potential field, one can estimate the smallness of gradients by examining whether any two spatially close obstacles/boundaries have close potential values, but this procedure does not scale well upon increasing the number of obstacles. Given a fast potential solver, a more practical strategy is to try a few boundary placements and double check the feasible paths that are found. For the configuration given in Fig. 5(a), placing two parallel boundaries tilted at 45° [Fig. 5(d)] also finds three topologically non-equivalent paths comparable to those shown in Fig. 5(c). Thus the proposed scheme can be made robust against small gradients with one or two additional calculations. In this case the computational times listed in the last column of Table 1 are accordingly increased by about 50%.

C. COMPARISON TO THE POTENTIAL FIELD APPROACH

We now pinpoint the differences between our method and the Potential Field approach [17], [18], [19], [20], [21], [22] since both methods involve a potential field. The Potential Field approach regards each obstacle as a short-ranged repulsive potential and introduces a smooth potential that has a higher value at initial point and a lower value at the target point. The feasible path follows the gradient of the combined potential. Because the combined potential is *not* the solution of Laplace equation, there can be local minima or saddle points that trap the path from reaching the target point. A closely related concept is the navigation function (Chapter 8 of [38]) that can be regarded as a potential field with only one global minimum at the target point. If identified, the feasible path can always be constructed by following the gradient. However a formal construction of the navigation function needs to take actions into account and is very computationally demanding.

Our scheme regards each obstacle as a charge neutral conductor and the potential is found by *solving* a map-specific electrostatic problem. Using (F3) described in Section IV-C, a finite portion of path in our scheme follows the equipotential curve that is *perpendicular to* the gradient of potential field. This is fundamentally different from the way the Potential Field or the navigation function approach utilizes its potential field.

Our potential can be regarded as a compromise between the Potential Field approach and the navigation function:

Compared to the Potential Field approach, our potential has no vanishing gradients in $\mathcal{D}_{\text{ROI}}$ which guarantees the success of a gradient-based search, but it takes more effort to construct; Compared to navigation function, our potential is less informative since the target point is not an extreme point, but is much easier to construct using our developed solver. Finally the potential field in our scheme does not depend on the initial and target points, and a single potential calculation can be used to identify multiple paths.

VII. SIMULATION

In this section we provide two examples to illustrate our path generation scheme. The maps are chosen such that feasible paths are very different from straight lines connecting the initial and target points. Paths generated using the RRT, PRM, and Bug algorithms [23] are provided for comparison. The stepsize $\mathrm{d}Z = 0.1$ [Eq. (6)] has been used in these calculations.

A. NARROW-GAP SCENARIO

Fig. 6(a) shows the narrow-gap scenario. The planning problem is specified by

$$\begin{aligned} Z_{\text{init}} &= -1 - 0.5i;\ Z_{\text{target}} = 1 + 0.5i \\ \text{boundary 1 (line)} &= [-3 + i, +3 + i] \\ \text{boundary 2 (line)} &= [-3 - i, +3 - i] \\ \text{obstacle 1 (rect.)} &= [-2.2 - 0.3i, -0.2 + 0.3i] \\ \text{obstacle 2 (rect.)} &= [0.2 - 0.3i, 2.2 + 0.3i] \\ \text{region of interest (rect.)} &= [-2 - 2i, +2 + 2i]. \end{aligned} \tag{10}$$

The boundaries comprise two horizontal lines which are each specified by two endpoints. Two rectangular obstacles are specified by the coordinates of their diagonal vertices. The "region of interest" is chosen to be rectangular and is also specified by its diagonal vertices. We put -1 charge on (top) boundary 1, and +1 charge on (bottom) boundary 2. The resulting potential distribution is plotted in Fig. 6(a). The resulting potentials at initial/target points, boundaries and obstacle centers are:

$$\begin{aligned} \Phi_{\text{init}} &= -\Phi_{\text{target}} = 0.337 \\ \Phi_{\text{b},1} &= -1.178, \quad \Phi_{\text{b},2} = 1.178 \\ \Phi_{\text{obs},1} &= \Phi_{\text{obs},2} = 0. \end{aligned} \tag{11}$$

Fig. 6(c) shows the paths parameterized by potentials $\Phi_{\text{ref}} = \pm 0.1$. Passage through the narrow gap is achieved by the "downstream" part which connects Z_{init} and $Z_{\text{ref},1}$. To illustrate this point, we plot the positions of $Z_{\text{ref},1}$ and $Z_{\text{ref},2}$ [see Step 4 in Section V-A] for a feasible path of $\Phi_{\text{ref}} = +0.1$ and observe that it is the "downstream" part of the path (i.e. between Z_{init} and $Z_{\text{ref},1}$) that accounts for gap passage.

B. 3-BOXES SCENARIO

Fig. 6(b) shows the 3-boxes scenario, where

TABLE 1. Comparison on computation time.

Scenario	RRT (ave)	PRM (ave)	Bug	Proposed
narrow-gap	0.07 sec	0.20 sec	< 0.01 sec	0.07 sec
3-boxes	0.11 sec	0.26 sec	< 0.01 sec	0.10 sec

$$\begin{aligned} \text{boundary 1 (line)} &= [-2 + 1.5i, +2 + 1.5i] \\ \text{boundary 2 (line)} &= [-2 - 1.5i, +2 - 1.5i] \\ \text{obstacle 1 (rect.)} &= [-0.8 + 0.3i, +0.8 + 1.1i] \\ \text{obstacle 2 (rect.)} &= [-0.25 - 0.25i, +0.25 + 0.25i] \\ \text{obstacle 3 (rect.)} &= [-1. - 1.3i, +1. - 0.3i] \\ \text{region of interest (rect.)} &= [-2 - 1.5i, +2 + 1.5i]. \end{aligned} \tag{12}$$

We put -1 charge on (top) boundary 1 and $+1$ charge on (bottom) boundary 2 to solve for the electrostatic potential field, which is plotted in Fig. 6(b). The potentials at initial/target points, boundaries and obstacle centers are respectively

$$\begin{aligned} \Phi_{\text{init}} &= \Phi_{\text{target}} = 0.277 \\ \Phi_{\text{b},1} &= -1.472, \quad \Phi_{\text{b},2} = 1.401 \\ \Phi_{\text{obs},1} &= -0.168 \quad \Phi_{\text{obs},2} = 0.275, \quad \Phi_{\text{obs},3} = 0.719. \end{aligned} \tag{13}$$

Fig. 6(d) shows the feasible paths parameterized by potentials $\Phi_{\text{ref}} = 1, 0.5, 0, -1$. These four representative paths reach the target point via traversing four different gaps between boundaries and boxes. In this example, passing through a horizontal gap is done by following an equipotential curve. To illustrate this point, we plot the positions of $Z_{\text{ref},1}$ and $Z_{\text{ref},2}$ [see Step 4 in Section V-A] for the feasible path of $\Phi_{\text{ref}} = -1$ and see that it is the "equipotential" part of the path (between $Z_{\text{ref},1}$ and $Z_{\text{ref},2}$) that accounts for the horizontal path segment.

C. COMPARISONS WITH RRT, PRM, AND BUG ALGORITHMS

Feasible paths are generated by using RRT, PRM, and Bug algorithms. The results of RRT and Bug are shown in Fig. 6(e) and (f); those of PRM in Fig. 6(g) and (h). For the Bug algorithm we adopt a variant "Bug 1" where the bug leaves an obstacle at the point of its perimeter closest to the target point. Using a knowledge of the obstacle's surface, one could, in this case, skip the step to go around the whole obstacle to identify that perimeter point. For both the RRT and the Bug schemes we use a stepsize of $\lesssim 0.1$. Implementing PRM requires sampling nodes in the collision-free space and a roadmap that specifies the connections between sampling nodes. We use 200 and 100 points in $\mathcal{D}_{\text{ROI}}$ for the narrow-gap and 3-boxes scenarios, respectively, and it takes 286 and 136 random samplings to achieve the results shown in Fig. 6(g) and (h). When building the roadmap we keep 10 edges (nearest neighbors) for each sampling node.

All three methods find feasible paths. In Fig. 6(f) and (h) we purposely enlarge the middle box to close the narrow gaps between boxes; this forces the RRT, PRM and Bug schemes

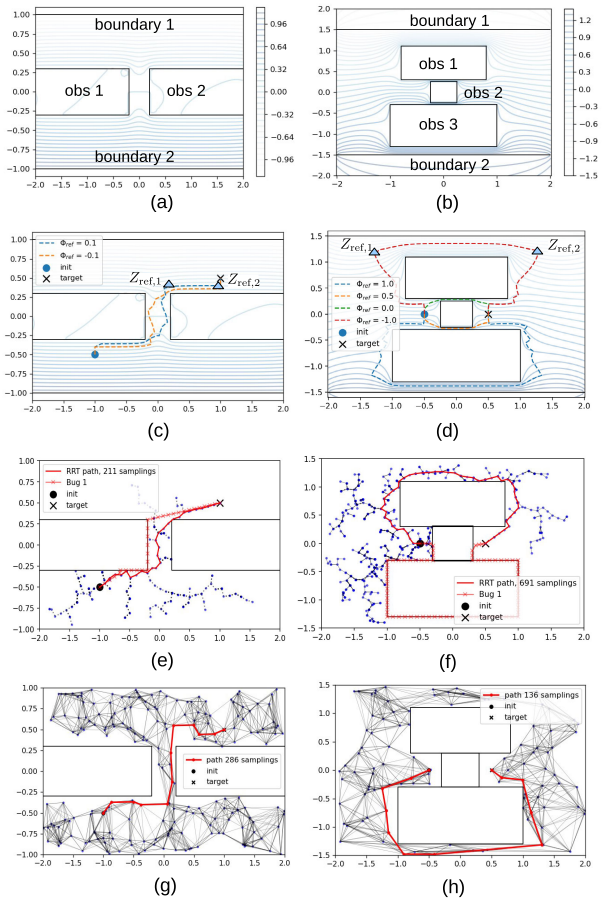

FIGURE 6. Path generation for narrow gap scenario (a), (c), (e), (g) and 3-boxes scenario (b), (d), (f), (h). (a) and (b): the potential. "obs" represents the obstacle. Charges of -1 and +1 are respectively placed on boundary 1 and boundary 2. (c) and (d): feasible paths generated by the proposed scheme. The curve between $Z_{\mathrm{ref},1}$ and $Z_{\mathrm{ref},2}$ represent the "equipotential" of a feasible path. (e) and (f): paths generated by RRT and Bug 1. (g) and (h): paths generated by PRM. In (f), (h) we purposely increase the size of mid box to eliminate narrow gaps between boxes.

to go around the top or bottom box. If there is a narrow gap, as in Fig. 6(d), all schemes can find the feasible path through one of the narrow gaps. In terms of the time to construct a path, the Bug algorithm is the fastest among all schemes. This is because Bug follows either a straight line or the perimeter of an obstacle. The former is very easy to construct and the latter is already known. The proposed scheme and RRT are comparable in speed. Usually the proposed method appears slightly faster, but RRT is stochastic so its computation time varies. PRM is slightly slower than both RRT and the proposed scheme. Table 1 summarizes the time taken (for RRT and PRM, the average time over 50 Monte Carlo runs are reported) to construct paths using different schemes. A CPU with 3.00 GHz Processor Base Frequency is used. Our method becomes significantly more time-efficient when the task involves generating multiple paths of different initial/target points.

In terms of the smoothness of the path, the Bug algorithm is as smooth as the obstacle shape except at a few sharp turns where the path goes from the straight line to the

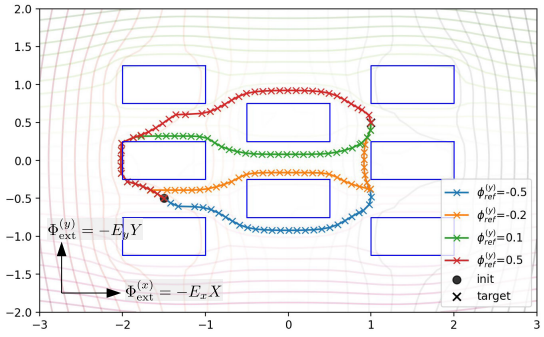

FIGURE 7. Path generation based on two orthogonal external electric fields. Eight rectangles represent the obstacles. Two sets of potentials $(\Phi_{\mathrm{tot}}^{(x)}, \Phi_{\mathrm{tot}}^{(y)})$, one corresponding to the uniform field along x and the other y, are obtained from the 2D potential solver. A feasible path can be labeled by either $\Phi_{\mathrm{ref}}^{(x)} = \Phi_{\mathrm{tot}}^{(x)}(X, Y)$ or $\Phi_{\mathrm{ref}}^{(y)} = \Phi_{\mathrm{tot}}^{(y)}(X, Y)$; here the latter is used. Four topologically non-equivalent paths are shown.

obstacle perimeter or vice versa. RRT and PRM paths are fragmented due to their random nature. The proposed scheme is in between. The path is mostly smooth except for two sharp turns between the equipotential part and the upstream/downstream parts. There may also be some small fluctuations when going around an obstacle due to the procedure shown in Fig. 4 (ii-b). Compared to the Bug algorithm, our scheme provides a different criterion for leaving an obstacle, guided by the potential. Compared to PRM, solving for the potential $\Phi(Z)$ corresponds to the roadmap construction phase, while following the equipotential (including the upstream and the downstream path) is analogous to the query phase of PRM.

The main advantage of the proposed scheme is the ability to generate multiple topologically non-equivalent paths from a single electrostatic calculation. In a sense, the Bug algorithm is fast in generating one feasible path because it only cares about the obstacles between the initial and target points. All other obstacles do not play any role in the path generation. RRT and PRM stochastically explore the entire allowed space and thus spend some time wandering around. The established tree is certainly useful for searching a path that has to pass some specified middle points. In our scheme, the feasible path is parameterized by the potential Φ_{ref}. By sampling or simply scanning a few Φ_{ref}'s, multiple feasible paths can be readily generated. The ability to generate multiple paths comes from the global information quantitatively encoded in the potential distribution. In any case, a hybrid of this type is expected to be useful for some applications.

VIII. EXTENSIONS

In this section we consider two alternatives for setting up boundary conditions that can be useful for task-specific applications.

A. EXTENSION 1: USE OF TWO EXTERNAL FIELDS

In auxiliary electrostatic problems considered so far, the charged objects are the sources of the spatially-varying potential field. This is not essential and an external electric

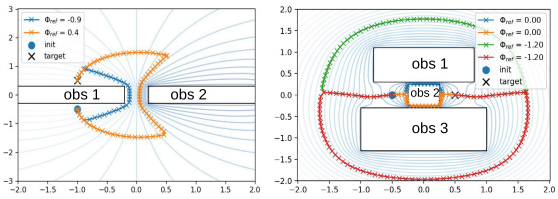

FIGURE 8. (a) For narrow-gap configuration [Fig. 6(a)], placing charges on obstacle 1 facilitates generating paths that avoid obstacle 1. (b) For the 3-boxes configuration [Fig. 6(b)], placing charges on obstacle 2 facilitates generating paths that avoid obstacle 2.

field can serve the same purpose. An illustrating example is given in Fig. 7. Like previous examples eight rectangular obstacles are represented by charge-neutral conductors, but unlike previous examples there are no boundaries with non-zero net charges. Instead, two orthogonal electric fields are applied. For the electric fields uniformly applied along the x and y directions, the external potentials are given by $\Phi^{(x)}_{\rm ext} = -E_x X$ and $\Phi^{(y)}_{\rm ext} = -E_y Y$, respectively, based on which we get potential fields $\Phi^{(x)}_{\rm tot}(Z)$ and $\Phi^{(y)}_{\rm tot}(Z)$. E_x and E_y can be arbitrary and are chosen to be one in Fig. 7. With two sets of potential fields, a feasible path can be labeled by either $\Phi^{(x)}_{\rm ref} = \Phi^{(x)}_{\rm tot}(Z)$ or $\Phi^{(y)}_{\rm ref} = \Phi^{(y)}_{\rm tot}(Z)$ and can be constructed as follows. For a given initial point $Z_{\rm init}$ and a target point $Z_{\rm target}$, a feasible path, labeled by $\Phi^{(y)}_{\rm ref}$, is generated by concatenating three arcs:

$$Z_{\rm init} \underset{\rm (i)}{\rightarrow} Z_{{\rm ref},1} \underset{\rm (ii)}{\rightarrow} Z_{{\rm ref},2} \underset{\rm (iii)}{\rightarrow} Z_{\rm target}, \tag{14}$$

where arc (i) is determined by $\Phi^{(x)}_{\rm tot}(Z_{\rm init}) = \Phi^{(x)}_{\rm tot}(Z_{{\rm ref},1})$; arc (ii) by $\Phi^{(y)}_{\rm tot}(Z_{{\rm ref},1}) = \Phi^{(y)}_{\rm tot}(Z_{{\rm ref},2}) = \Phi^{(y)}_{\rm ref}$; arc (iii) by $\Phi^{(x)}_{\rm tot}(Z_{{\rm ref},2}) = \Phi^{(x)}_{\rm tot}(Z_{\rm target})$. Eq. (14) is analogous to Steps 4-5 in Alg. 1; the only difference is that the downstream/upstream arcs in Alg. 1 are replaced by the equipotential curves of the potential field caused by the orthogonal applied field. In Fig. 7, we use $\Phi^{(y)}_{\rm ref}$ to label feasible paths and four topologically non-equivalent paths are shown. Removing the boundaries reduces the dimension of the electrostatic problem (see Appendix) and thus shortens the time to obtain the potential; the price to pay is that we need to solve for at least two potential fields, corresponding to two linearly independent applied electric fields, in order to construct feasible paths. Depending on the applications, this option can be beneficial.

B. EXTENSION 2: TASK SPECIFIC CHARGE ASSIGNMENT

We now explore the "charge" degree of freedom. When the goal of the feasible path is to go from one side to the other side of one specific obstacle, we could put a net charge *only* on that obstacle so that all equipotential contours enclose that obstacle. Following equipotentials is the easier part within our scheme. With this heuristic based on electrostatics, we reconsider the examples shown in Fig. 6. In Fig. 8(a) which represents the narrow-gap configuration [Fig. 6(a)], placing charges on obstacle 1 facilitates generating paths that avoid obstacle 1. In Fig. 8 (b), which represents the 3-boxes configuration [Fig. 6(b)], placing charges on obstacle 2 facilitates generating paths that avoid obstacle 2. Comparing Fig. 8(a) and (b) to their counterparts in Fig. 6(a) and (b), the former has two numeric advantages. First, two line boundaries are removed, which reduces the computational time to obtain the 2D potential. Second the majority of the feasible paths follow an equipotential curve which is easier to construct. However, we must bear in mind that placing net charge on the obstacle results in local extrema in the region of interest and can potentially ruin the path construction; we suggest that one should avoid placing non-zero charges on more than two obstacles.

IX. CONCLUSION

Path planning is a classical problem in robotics and an active area of research in autonomous driving, manipulation, etc. In this paper, we proposed a resolution-complete method to generate feasible paths in obstacle-cluttered 2D environments that involves solving for a 2D electrostatic potential. In our proposed method, all obstacles are represented by conductors of zero total charges whereas two boundaries are two metallic curves having different amounts of net charge. The electrostatics demand a constant potential for the surface of each obstacle, and therefore a feasible trajectory that avoids *all* obstacles can be generated by following the equipotential curve whose potential value is different from those of obstacles. In this manner each feasible path is associated with its potential value and one can in principle generate an infinite number of feasible paths.

The most distinct feature brought by our method is the quantitative use of global information – the obstacles and boundaries far away affect the equipotential curves at a given local point via the 2D long-ranged Coulomb interaction. Upon solving the 2D electrostatic potentials, all obstacles and boundaries affect one another. By following the equipotential curve the distant information influences the local path planning. The most critical step of our scheme is to accurately and rapidly solve the 2D potential, and we develop a very effective 2D potential solver utilizing the analytical properties of complex functions to fulfill this demanding task. A different look at a classic problem can bring new heuristics. In this case, intuition about electric fields can be helpful. The proposed path generation scheme provides a novel and quantitative device to encode the global information that can be complementary to existing methods.

APPENDIX
ELECTROSTATIC POTENTIAL SOLVER

The proposed 2D electrostatic potential solver, including its benchmarking and convergence, is detailed below.

A. ADAPTIVE REAL-SPACE EXPANSION OF POTENTIAL

To obtain the electrostatic potential for systems composed of 2D metallic objects, one needs to specify the surface of each

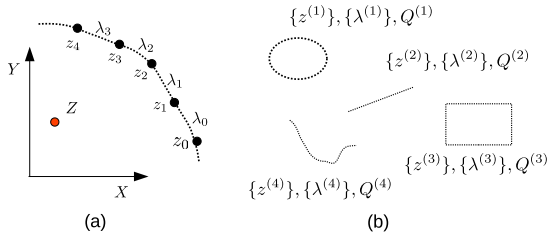

FIGURE 9. (a) Parametrization of the metallic surface by $\{z_i\}$ and the corresponding surface charge density by $\{\lambda_i\}$. (b) A collection of metallic surfaces and the corresponding surface charge densities.

object. We define the following parameters for the metallic surface locations $z_i^{(n)}$ and charge densities $\lambda_i^{(n)}$ of object n:

$$\begin{aligned} z^{(n)}(s) &\to \{z_i^{(n)}\} = (z_0^{(n)}, \cdots, z_{N^{(n)}}^{(n)}) \\ &\to \{\bar{z}_i^{(n)}\} = \Big(\frac{z_0^{(n)}+z_1^{(n)}}{2}, \cdots, \frac{z_{N^{(n)}-1}^{(n)}+z_{N^{(n)}}^{(n)}}{2}\Big) \\ \lambda^{(n)}(s) &\to \{\lambda_i^{(n)}\} = (\lambda_1^{(n)}, \lambda_2^{(n)}, \cdots, \lambda_{N^{(n)}}^{(n)}) \\ \mathrm{d}z^{(n)}(s) &\to \{\mathrm{d}z_i^{(n)}\} = (\mathrm{d}z_1^{(n)}, \cdots, \mathrm{d}z_{N^{(n)}}^{(n)}) \\ &\equiv \big(z_1^{(n)} - z_0^{(n)}, \cdots, z_{N^{(n)}}^{(n)} - z_{N^{(n)}-1}^{(n)}\big). \end{aligned} \tag{15}$$

Here $z^{(n)}(s)$ describes the nth metallic surface (i.e., the boundary of nth metallic object) with s a continuous parameter of a curve. In practice we use a set of discrete points $\{z_i^{(n)}\}$ ($i = 0$ to $N^{(n)}$) to represent the nth metallic surface (s is replaced by the subscript i); $\lambda_i^{(n)}$ ($i = 1$ to $N^{(n)}$) is the corresponding surface charge density at $\bar{z}_i^{(n)} = \frac{1}{2}(z_i^{(n)} + z_{i+1}^{(n)})$ [see Fig. 9(a) for illustration]. $\{\mathrm{d}z_i^{(n)}\}$ ($i = 1$ to $N^{(n)}$) is the difference between adjacent points which will be used later.

Following [35], the potential at a field point Z caused by a segment from z_1 to z_2 with line charge density λ is given by

$$\begin{aligned} &W_E(Z \mid z_1, z_2) \\ &= -2\lambda\Big[h(z_1 - Z) - h(z_2 - Z)\Big] \times \frac{|z_2 - z_1|}{z_2 - z_1} \\ &+ \text{const.}(z_1, z_2) \\ &= -\frac{2|z_2 - z_1|}{z_2 - z_1}\lambda\Big[\Big(Z - \frac{z_1+z_2}{2}\Big)\cdot\log\Big(\frac{z_2 - Z}{z_1 - Z}\Big) \\ &- \frac{z_2 - z_1}{2}\log\big[(z_2 - Z)(z_1 - Z)\big] + (z_2 - z_1)\Big] \\ &\equiv -\lambda\phi_r(Z \mid z_1, z_2). \end{aligned} \tag{16}$$

In the first equality $h(r) = r\log[r]$. $\phi_r(Z \mid z_1, z_2)$ will be referred to as the potential basis function. The second equality of Eq. (16) ensures an integration constant consistent with

$$\mathrm{Re}\big[W_E(Z \mid z_1, z_2)\big] = 2\lambda\int_0^{|z_2 - z_1|} \mathrm{d}t\ \log(|\, Z - z(t)\,|), \tag{17}$$

where $z(t) = z_1 + t\frac{z_2 - z_1}{|z_2 - z_1|}$. The single-valued potential is given by $\Phi = -\mathrm{Re}[W_E]$. $\mathrm{Im}[W_E]$ has no physical meaning.

With Eqs. (15) and (16), the superposition principle demands that the potential at location Z generated by the nth surface be

$$\Phi_{\text{ind}}^{(n)}(Z \mid \{z_i^{(n)}\}, \{\lambda_i^{(n)}\}) = \sum_{i=1}^{N^{(n)}} \lambda_i^{(n)}\phi_r(Z \mid z_i^{(n)}, z_{i+1}^{(n)}). \tag{18}$$

The overall induced potential $\Phi_{\text{ind}} = \sum_n \Phi_{\text{ind}}^{(n)}$, and the total potential includes the contribution from any external field. The complex electric field corresponding to the gradient of the potential generated by nth surface is [35]

$$\begin{aligned} &\overline{E}_{\text{ind}}^{(n)}(Z \mid \{z_i^{(n)}\}, \{\lambda_i^{(n)}\}) \\ &= \sum_{i=1}^{N^{(n)}} 2\lambda_i^{(n)} B_r(Z \mid z_i^{(n)}, z_{i+1}^{(n)}) = E_X - iE_Y, \\ &\text{where } B_r(Z \mid z_1, z_2) = \frac{|\, z_2 - z_1\,|}{z_2 - z_1}\log\Big[\frac{z_1 - Z}{z_2 - Z}\Big] \end{aligned} \tag{19}$$

and the total induced electric field is the summation over all surfaces. The total electric field must include the external contribution.

B. SELF-CONSISTENCY FROM ENERGY MINIMIZATION

Eq. (18) and (19) always represent solutions for the electrostatic potential and field corresponding to some boundary condition, and the task now is to find the coefficients that corresponds to the case of interest. This will be done by minimizing the total electric energy with constraints that the total charge on each metallic object is fixed.

Let us first specify the constraint. Assume the total charge on nth surface is $Q^{(n)}$, the charge constraint using Eq. (15) can be expressed as

$$Q^{(n)} = \int \mathrm{d}s\lambda^{(n)}(s) \to \sum_{i=1}^{N^{(n)}} \lambda_i^{(n)}\,|\mathrm{d}z_i^{(n)}|. \tag{20}$$

For M metallic surfaces, the surface charge distribution can be obtained by minimizing the total energy:

$$\begin{aligned} E_{\text{tot}} &= \frac{1}{2}\int \mathrm{d}\mathbf{r}\,\rho(\mathbf{r})\Phi_{\text{ind}}(\mathbf{r}) + \int \mathrm{d}\mathbf{r}\,\rho(\mathbf{r})\Phi_{\text{ext}}(\mathbf{r}) \\ &\to \frac{1}{2}\sum_{m=1}^{M}\sum_{i=1}^{N^{(m)}} |\mathrm{d}z_i^{(m)}|\lambda_i^{(m)}\Big[2\Phi_{\text{ext}}(\bar{z}_i^{(m)}) \\ &+ \sum_{m'=1}^{M}\Phi_{\text{ind}}^{(m')}(\bar{z}_i^{(m)})\Big] \end{aligned} \tag{21}$$

The induced potential comes from all M metallic surfaces. Using Eq. (18), we have the final expression:

$$\begin{aligned} E_{\text{tot}} &= \sum_{m=1}^{M}\sum_{i=1}^{N^{(m)}} \lambda_i^{(m)} V_{m,i} \\ &+ \frac{1}{2}\sum_{m=1}^{M}\sum_{i=1}^{N^{(m)}}\sum_{m'=1}^{M}\sum_{i'=1}^{N^{(m')}} \lambda_i^{(m)}\lambda_{i'}^{(m')} P_{m,i;m',i'} \end{aligned} \tag{22a}$$

$$V_{m,i} = |\mathrm{d}z_i^{(m)}| \cdot \Phi_{\text{ext}}(\bar{z}_i^{(m)}) \tag{22b}$$

$$P_{m,i;m',i'} = |\mathrm{d}z_i^{(m)}| \cdot \phi_r(\bar{z}_i^{(m)} \mid z_{i'}^{(m')}, z_{i'+1}^{(m')}) \tag{22c}$$

There are M constraints for total charges

$$\sum_{i=1}^{N^{(m)}} \lambda_i^{(m)} |\mathrm{d}z_i^{(m)}| = Q^{(m)}, \text{ for } m = 1 \ldots M. \tag{23}$$

Minimizing Eq. (22a) with equality constraints (23) is a standard quadratic programming (QP) optimization. We use OSQP [51] as the solver. Some numerical issues with the optimization process will be discussed in Section D. Here we point out that specifying $P_{m,i;m',i'}$ takes more than 95% of the calculation time, and it is the most time-consuming part of our path generating scheme.

C. CONVERGENCE CRITERION AND TWO EXAMPLES

For systems of metallic surfaces, the tangential component of electric field at the surfaces has to vanish (otherwise the charges will move), so the smallness of the following quantity

$$\begin{aligned} E[\{\lambda_i^{(n)}\}] &= \sum_n \int \mathrm{d}s\, |E_t(z^{(n)}(s), \{\lambda_i^{(n)}\})|^2 \\ &\approx \sum_n \sum_i \mathrm{d}z_i^{(n)}\, |E_t(z_i^{(n)}, \{\lambda_i^{(n)}\})|^2, \\ &\text{where } z_i^{(n)} \in n\text{th surface}, \end{aligned} \tag{24}$$

can be used to quantify the discretization error. In Eq. (24) $\lambda_i^{(n)}$ is the solution and E_t the tangential component of the electric field at the surface which is determined from Eq. (19). The magnitude of the transverse electric field also indicates the locations where more points are needed if a solution of higher accuracy is required.

Two simple examples are provided to illustrate the effectiveness of the solver. The first example is a charge-neutral unit circle in a uniform electric field $\mathbf{E}_{\text{ext}} = \hat{x}$ so the external potential $\Phi_{\text{ext}} = -x$. Fig. 10(a) clearly shows the expected screening effect (a constant potential inside the circle). The induced surface charge in this case has an analytical expression $\rho(\theta) = \frac{1}{2\pi}\cos\theta$ where $\theta = 0$ defines $\hat{x}$. Fig. 10(b) shows that using merely 20 points to represent the circle already gives a very good result, which is modestly improved by using 50 points. Fig. 10(c) shows that the tangential component of electric field decreases in amplitude upon increasing the number of points. A more subtle case is a 1 cm segment carrying 1 StatC charge: the ends of a line represent the sharpest boundaries one could have and are expected to cause some divergent behavior. As shown in Fig. 10(e), the converged surface charge density indeed diverges at both ends. Upon increasing the number of points parameterizing the line, the tangential component of electric field becomes smaller but its magnitude still blows up around the ends of the line [Fig. 10(f)]. Despite these divergences, the equipotential curves shown in Fig. 10(d) are reasonable in the sense that the shapes of contours are elongated along x to comply with the shape of the line, although some of them actually cross the line. The results of using 10 points and 100 points are only visibly different close to two ends

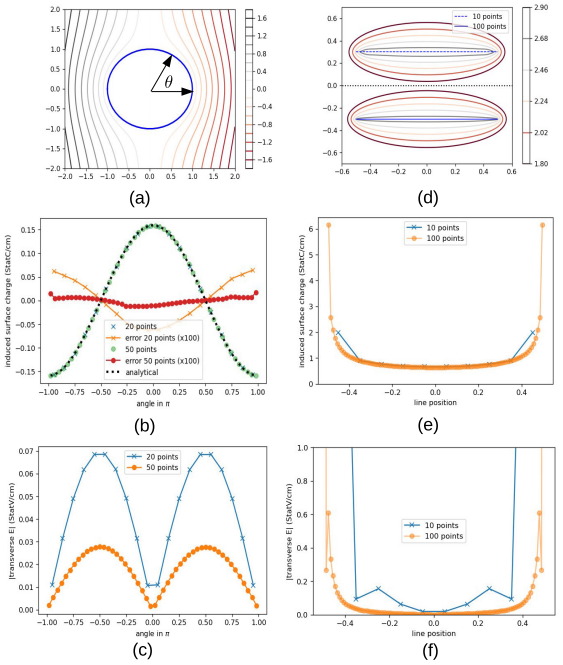

FIGURE 10. Analysis of a 2D circle (a)-(c) and a charged line (d)-(e). (a) The equipotential curves of a charge neutral circle of radius 1 cm in a uniform field $\mathbf{E} = +\hat{x}$. (b) The induced surface charges using 20 and 50 points. The differences (multiplied by 100) from the analytical results are also shown. (c) The strength of the transverse field on the circle. (d) The equipotential curves of a 1 cm line segment carrying 1 StatC charge: top for using 10 points and bottom for using 100 points. Their difference is only visible for contours very close to the line segment. (e) The induced surface charges using 10 and 100 points. (f) The strength of the transverse field on the line.

of the segment [see the contour of potential value 2.9 in the top and bottom of Fig. 10(d)]. In that case the contour using 100 points conforms more closely to the line shape. This nice property turns out to be beneficial for the path generation discussed in the main text.

D. REMARKS ON THE POTENTIAL SOLVER

We conclude by a few general remarks about the proposed potential solver. First, our solver solves for a 2D potential by determining a 1D charge distribution and thus offers a memory-efficient representation of the solution. The rationale behind the expansion is to fully respect that the non-smoothness of the potential and electric field originates *solely* from the induced charges at the metallic surfaces. The chosen (non-orthogonal) basis functions [both Eqs. (18) and (19)] not only satisfy the Laplace equation but also accurately capture the non-smoothness across the charged boundary as they are the integrated results of Coulomb's law [35].

Second, determining the induced charges by minimizing the total electric energy is a realization of a variational principle – one tries to find the best charge distribution for a given energy functional. As our solver enforces the non-smoothness across the metallic surfaces, the resulting potential always reflects the surface shape even for a rough discretization. This is seen in Fig. 10(d) where contours close

to the line are strongly stretched along x to conform to the line shape.

Third, expressing the potential as an expansion allows computing the potential at any point in the 2D plane. The gradient (i.e., electric field) computed by Eq. (19) corresponds exactly to the potential without any interpolation errors. In other words, the discretization errors for potential and its gradient are consistent to preserve $-\nabla\Phi_{\text{tot}} = \mathbf{E}_{\text{tot}}$. Computation complexities for evaluating the potential and the gradient are the same. This property is useful for constructing the equipotential curves.

Finally, we point out an issue we have encountered regarding QP optimization. From the physics point of view, the P matrix in Eq. (22a) corresponds to capacitance and should be positive definite. When the surfaces include sharp edges, however, the P matrix usually (not always, but we do not have control) develops a negative eigenvalue that rules out a few QP solvers [52], [53], [54]. The negative eigenvalue goes away when projecting the P matrix into the null space of the linear equality constraints (23), meaning that a global minimum exists in the space allowed by the constraints. We use OSQP [51] as the QP solver because it can deal with the non-positive eigenvalues of P in a robust manner.

ACKNOWLEDGMENT

The authors would like to thank Dr. Arvind Raghunathan (MERL) for very insightful suggestions on the QP solver and Dr. Siddarth Jain (MERL) for helpful discussion about the PRM implementation.

REFERENCES

[1] D. Dolgov, S. Thrun, M. Montemerlo, and J. Diebel, "Path planning for autonomous driving in unknown environments," in *Experimental Robotics*, O. Khatib, V. Kumar, and G. J. Pappas, Eds. Berlin, Germany: Springer, 2009, pp. 55–64.

[2] K. Chu, M. Lee, and M. Sunwoo, "Local path planning for off-road autonomous driving with avoidance of static obstacles," *IEEE Trans. Intell. Transp. Syst.*, vol. 13, no. 4, pp. 1599–1616, Dec. 2012.

[3] M. N. A. Wahab, S. Nefti-Meziani, and A. Atyabi, "A comparative review on mobile robot path planning: Classical or meta-heuristic methods?" *Annu. Rev. Control*, vol. 50, pp. 233–252, Jan. 2020. [Online]. Available: https://www.sciencedirect.com/science/article/pii/S1367578820300675

[4] A. Stentz and I. C. Mellon, "Optimal and efficient path planning for unknown and dynamic environments," *Int. J. Robot. Automat.*, vol. 10, pp. 89–100, Aug. 1993.

[5] D. Hsu, R. Kindel, J.-C. Latombe, and S. Rock, "Randomized kinodynamic motion planning with moving obstacles," *Int. J. Robot. Res.*, vol. 21, no. 3, pp. 233–255, Mar. 2002.

[6] S. M. LaValle and J. J. Kuffner Jr., "Randomized kinodynamic planning," *Int. J. Robot. Res.*, vol. 20, no. 5, pp. 378–400, 2001.

[7] S. Karaman and E. Frazzoli, "Sampling-based algorithms for optimal motion planning," *Int. J. Robot. Res.*, vol. 30, no. 7, pp. 846–894, Jun. 2011.

[8] D. Ferguson and A. Stentz, "Anytime RRTs," in *Proc. IEEE/RSJ Int. Conf. Intell. Robots Syst.*, Oct. 2006, pp. 5369–5375.

[9] J. M. Pimentel, M. S. Alvim, M. F. M. Campos, and D. G. Macharet, "Information-driven rapidly-exploring random tree for efficient environment exploration," *J. Intell. Robotic Syst.*, vol. 91, no. 2, pp. 313–331, Aug. 2018.

[10] D. Connell and H. M. La, "Extended rapidly exploring random tree-based dynamic path planning and replanning for mobile robots," *Int. J. Adv. Robotic Syst.*, vol. 15, no. 3, 2018, Art. no. 1729881418773874.

[11] Y. Wang, D. K. Jha, and Y. Akemi, "A two-stage RRT path planner for automated parking," in *Proc. 13th IEEE Conf. Autom. Sci. Eng. (CASE)*, Aug. 2017, pp. 496–502.

[12] L. E. Kavraki, P. Svestka, J.-C. Latombe, and M. H. Overmars, "Probabilistic roadmaps for path planning in high-dimensional configuration spaces," *IEEE Trans. Robot. Autom.*, vol. 12, no. 4, pp. 566–580, Aug. 1996.

[13] E. W. Dijkstra, "A note on two problems in connexion with graphs," *Numerische Math.*, vol. 1, no. 1, pp. 269–271, Dec. 1959.

[14] M. Noto and H. Sato, "A method for the shortest path search by extended Dijkstra algorithm," in *Proc. IEEE Int. Conf. Syst., Man Cybern.*, vol. 3, May 2000, pp. 2316–2320.

[15] P. Sudhakara, V. Ganapathy, and K. Sundaran, "Probabilistic roadmaps-spline based trajectory planning for wheeled mobile robot," in *Proc. Int. Conf. Energy, Commun., Data Analytics Soft Comput. (ICECDS)*, Aug. 2017, pp. 3579–3583.

[16] N. Kumar, Z. Vámossy, and Z. M. Szabó-Resch, "Robot path pursuit using probabilistic roadmap," in *Proc. IEEE 17th Int. Symp. Comput. Intell. Informat. (CINTI)*, Nov. 2016, pp. 000139–000144.

[17] O. Khatib, "Real-time obstacle avoidance for manipulators and mobile robots," *Int. J. Robot. Res.*, vol. 5, no. 1, pp. 90–98, Mar. 1986.

[18] Y. Koren and J. Borenstein, "Potential field methods and their inherent limitations for mobile robot navigation," in *Proc. IEEE Int. Conf. Robot. Autom.*, vol. 2, Apr. 1991, pp. 1398–1404.

[19] Y. K. Hwang and N. Ahuja, "A potential field approach to path planning," *IEEE Trans. Robot. Autom.*, vol. 8, no. 1, pp. 23–32, Feb. 1992.

[20] F. Bayat, S. Najafinia, and M. Aliyari, "Mobile robots path planning: Electrostatic potential field approach," *Exp. Syst. Appl.*, vol. 100, pp. 68–78, Jun. 2018.

[21] S. M. H. Rostami, A. K. Sangaiah, J. Wang, and X. Liu, "Obstacle avoidance of mobile robots using modified artificial potential field algorithm," *EURASIP J. Wireless Commun. Netw.*, vol. 2019, no. 1, p. 70, Mar. 2019.

[22] U. Orozco-Rosas, O. Montiel, and R. Sepulveda, "Mobile robot path planning using membrane evolutionary artificial potential field," *Appl. Soft Comput.*, vol. 77, pp. 236–251, Apr. 2019.

[23] V. J. Lumelsky and A. A. Stepanov, "Path-planning strategies for a point mobile automaton moving amidst unknown obstacles of arbitrary shape," *Algorithmica*, vol. 2, nos. 1–4, pp. 403–430, Nov. 1987.

[24] N. Ulrich, *Mobile Robotics: A Practical Introduction*, 2nd ed. London, U.K.: Springer, 2003.

[25] R. Siegwart, I. R. Nourbakhsh, and D. Scaramuzza, *Introduction to Autonomous Mobile Robots* (Intelligent Robotics and Autonomous Agents Series), 2nd ed. Cambrdige, MA, USA: MIT Press, 2011.

[26] P. Hart, N. Nilsson, and B. Raphael, "A formal basis for the heuristic determination of minimum cost paths," *IEEE Trans. Syst. Sci. Cybern.*, vol. SSC-4, no. 2, pp. 100–107, Jul. 1968.

[27] M. Likhachev, G. Gordon, and S. Thrun, *ARA*: Anytime A* With Probable Bounds on Sub-Optimality*. Cambridge, MA, USA: MIT Press, 2003.

[28] S. Koenig, M. Likhachev, and D. Furcy, "Lifelong planning A*," *Artif. Intell.*, vol. 155, nos. 1–2, pp. 93–146, 2004.

[29] Y. Wang, "Improved A-search guided tree construction for kinodynamic planning," in *Proc. Int. Conf. Robot. Autom. (ICRA)*, May 2019, pp. 5530–5536.

[30] J. Leu, Y. Wang, M. Tomizuka, and S. Di Cairano, "Improved A-search guided tree for autonomous trailer planning," in *Proc. IEEE/RSJ Int. Conf. Intell. Robots Syst. (IROS)*, Oct. 2022, pp. 7190–7196.

[31] T. Lozano-Pérez and M. A. Wesley, "An algorithm for planning collision-free paths among polyhedral obstacles," *Commun. ACM*, vol. 22, no. 10, pp. 560–570, Oct. 1979.

[32] Y.-H. Liu and S. Arimoto, "Path planning using a tangent graph for mobile robots among polygonal and curved obstacles: Communication," *Int. J. Robot. Res.*, vol. 11, no. 4, pp. 376–382, Aug. 1992.

[33] N. Ratliff, M. Zucker, J. A. Bagnell, and S. Srinivasa, "CHOMP: Gradient optimization techniques for efficient motion planning," in *Proc. IEEE Int. Conf. Robot. Autom.*, May 2009, pp. 489–494.

[34] A. U. Raghunathan, D. K. Jha, and D. Romeres, "PYROBOCOP: Python-based robotic control & optimization package for manipulation and collision avoidance," 2021, *arXiv:2106.03220*.

[35] R. A. Beth, "Complex representation and computation of two-dimensional magnetic fields," *J. Appl. Phys.*, vol. 37, no. 7, pp. 2568–2571, Jun. 1966.

[36] R. A. Beth, "An integral formula for two-dimensional fields," *J. Appl. Phys.*, vol. 38, no. 12, pp. 4689–4692, Nov. 1967.

[37] J. H. Mathews and R. W. Howell, *Complex Analysis for Mathematics and Engineering*, 6th ed. Sudbury, MA, USA: Jones & Bartlett Publishers, 2012.
[38] S. M. LaValle, *Planning Algorithms*. Cambridge, U.K.: Cambridge Univ. Press, 2006.
[39] P. Tokekar, N. Karnad, and V. Isler, "Energy-optimal trajectory planning for car-like robots," *Auto. Robots*, vol. 37, no. 3, pp. 279–300, Oct. 2014, doi: 10.1007/s10514-014-9390-3.
[40] B. R. Donald and P. Xavier, "Provably good approximation algorithms for optimal kinodynamic planning: Robots with decoupled dynamics bounds," *Algorithmica*, vol. 14, no. 6, pp. 443–479, Dec. 1995.
[41] Y. Wang, K. Ueda, and S. A. Bortoff, "A Hamiltonian approach to compute an energy efficient trajectory for a servomotor system," *Automatica*, vol. 49, no. 12, pp. 3550–3561, Dec. 2013.
[42] Y. Wang, Y. Zhao, S. A. Bortoff, and K. Ueda, "A real-time energy-optimal trajectory generation method for a servomotor system," *IEEE Trans. Ind. Electron.*, vol. 62, no. 2, pp. 1175–1188, Feb. 2015.
[43] O. Wigstrom, B. Lennartson, A. Vergnano, and C. Breitholtz, "High-level scheduling of energy optimal trajectories," *IEEE Trans. Autom. Sci. Eng.*, vol. 10, no. 1, pp. 57–64, Jan. 2013.
[44] Y. Zhao and P. Tsiotras, "Analysis of energy-optimal aircraft landing operation trajectories," *J. Guid., Control, Dyn.*, vol. 36, no. 3, pp. 833–845, May 2013.
[45] T. Chettibi, H. E. Lehtihet, M. Haddad, and S. Hanchi, "Minimum cost trajectory planning for industrial robots," *Eur. J. Mech.-A/Solids*, vol. 23, no. 4, pp. 703–715, Jul. 2004.
[46] S. Björkenstam, D. Gleeson, R. Bohlin, J. S. Carlson, and B. Lennartson, "Energy efficient and collision free motion of industrial robots using optimal control," in *Proc. 9th IEEE CASE*, Madison, WI, USA, Aug. 2013, pp. 510–515.
[47] A. Richards, T. Schouwenaars, J. P. How, and E. Feron, "Spacecraft trajectory planning with avoidance constraints using mixed-integer linear programming," *J. Guid., Control, Dyn.*, vol. 25, no. 4, pp. 755–764, Jul. 2002.
[48] D. J. Griffiths, *Introduction to Electrodynamics*, 4th ed. Boston, MA, USA: Pearson, 2013.
[49] H. Prautzsch, W. Boehm, and M. Paluszny, *Bézier and B-Spline Techniques* (Mathematics and Visualization), 1st ed. Berlin, Germany: Springer, 2002.
[50] G. D. Knott, *Interpolating Cubic Splines* (Progress in Computer Science and Applied Logic), vol. 18. Basel, Switzerland: Birkhauser, 2000.
[51] B. Stellato, G. Banjac, P. Goulart, A. Bemporad, and S. Boyd, "OSQP: An operator splitting solver for quadratic programs," *Math. Program. Comput.*, vol. 12, no. 4, pp. 637–672, Dec. 2020, doi: 10.1007/s12532-020-00179-2.
[52] D. Goldfarb and A. Idnani, "A numerically stable dual method for solving strictly convex quadratic programs," *Math. Program.*, vol. 27, no. 1, pp. 1–33, Sep. 1983.
[53] E. D. Andersen, C. Roos, and T. Terlaky, "On implementing a primal-dual interior-point method for conic quadratic optimization," *Math. Program.*, vol. 95, no. 2, pp. 249–277, Feb. 2003.
[54] A. Domahidi, E. Chu, and S. Boyd, "ECOS: An SOCP solver for embedded systems," in *Proc. Eur. Control Conf. (ECC)*, Jul. 2013, pp. 3071–3076.

CHUNGWEI LIN received the B.S. degree from National Taiwan University, in 1997, the M.S. degree from Tsinghua University, in 1999, and the Ph.D. degree in physics from Columbia University, New York, NY, USA, in 2008.

He is currently a Principal Research Scientist with Mitsubishi Electric Research Laboratories, Cambridge, MA, USA. His research interests include condensed matter physics, superconducting technology, and quantum control.

YEBIN WANG (Senior Member, IEEE) received the B.Eng. degree in mechatronics engineering from Zhejiang University, Hangzhou, China, in 1997, the M.Eng. degree in control theory and control engineering from Tsinghua University, Beijing, China, in 2001, and the Ph.D. degree in electrical engineering from the University of Alberta, Edmonton, AB, Canada, in 2008.

From 2001 to 2003, he was a Software Engineer, the Project Manager, and the Manager of the Research and Development Department in automation industries. He has been with Mitsubishi Electric Research Laboratories, Cambridge, MA, USA, since 2009, where he is currently a Senior Principal Research Scientist. His research interests include nonlinear control and estimation, optimal control, adaptive systems, and their applications including mechatronic systems.

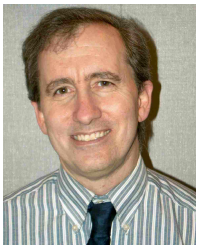

WILLIAM T. VETTERLING (Life Member, IEEE) received the B.A. degree in physics from Amherst College, in 1970, and the Ph.D. degree in solid-state physics from Harvard University, in 1976.

He was with the Physics Faculty, Harvard University, from 1976 to 1984. In 1984, he became a Principal Scientist with Polaroid Corporation, while remaining a Research Associate and a Visiting Lecturer with Harvard University. In 1998, he became a Distinguished Scientist, in 2003, a Science and Technology Fellow, and the Manager of the Polaroid Image Science Laboratory. In 2005, he became a Research Fellow with Zink Imaging, a Polaroid spin-off. He is the coauthor of the numerical recipes series of books and software from Cambridge University Press and the author of more than 50 research articles in solid state physics, image science, and numerical simulation. He is also a co-inventor of 50 U.S. patents.

DEVESH K. JHA (Senior Member, IEEE) received the M.S. degree in mechanical engineering and mathematics and the Ph.D. degree in mechanical engineering from The Pennsylvania State University, State College, PA, USA, in December 2016.

He is currently a Research Scientist with Mitsubishi Electric Research Laboratories (MERL), Cambridge, MA, USA. His research interests include machine learning, robotics, and deep learning. He was a recipient of several best paper awards, including the Kalman Best Paper Award from the Dynamic Systems and Control Division, American Society of Mechanical Engineers (ASME), in 2019.

RIEN QUIRYNEN received the bachelor's degree in computer science and electrical engineering and the master's degree in mathematical engineering from KU Leuven, Belgium, and the joint Ph.D. degree from KU Leuven, and the University of Freiburg, Germany. He received a four-year Ph.D. scholarship from the Research Foundation Flanders (FWO), from 2012 to 2016. He was a Senior Research Scientist with Mitsubishi Electric Research Laboratories, Cambridge, MA, USA, from early 2017 to late 2023. He is currently a Staff Software Engineer with Stack AV. He has authored/coauthored more than 75 peer-reviewed papers in journals and conference proceedings and 25 patents. His research interests include numerical optimization algorithms for decision making, motion planning, and predictive control of autonomous systems. He serves as an Associate Editor for the *Optimal Control Applications and Methods* (Wiley) and the IEEE CCTA Editorial Board.